2001

Study of Dynamics and Mechanism of Metal-Induced Silicon Growth

Elena A. Guliants
University of Dayton, eguliants1@udayton.edu

Wayne A. Anderson
State University of New York at Buffalo

Study of dynamics and mechanism of metal-induced silicon growth

Elena A. Guliants and Wayne A. Anderson
Department of Electrical Engineering, State University of New York at Buffalo, 212 Bonner Hall, Amherst, New York 14260

(Received 28 July 2000; accepted for publication 1 February 2001)

The present study addresses the mechanism of metal-induced growth of device-quality silicon thin films. Si deposition was performed by magnetron sputtering on a 25-nm-thick Ni prelayer at 525–625 °C and yielded a continuous, highly crystalline film with a columnar structure. A Ni disilicide intermediate layer formed as a result of the Ni reaction with Si deposit provides a sufficient site for the Si epitaxial growth because lattice mismatch is small between the two materials. The reaction between Ni and Si was observed to progress in several stages. The Ni_xSi_y phase evolution in a Ni:Si layer was studied by x-ray photoelectron spectroscopy, Auger electron spectroscopy, Rutherford backscattering spectrometry, transmission electron microscopy, and x-ray diffraction and found to be controlled by the Ni-to-Si concentration ratio at the growing front. After Ni is completely consumed in the silicide, continued Si deposition leads to the nucleation and growth of Si crystals on the surface of the $NiSi_2$ grains. The issues related to the nature of Ni_xSi_y phase transformations and Si heteroepitaxy are discussed. © *2001 American Institute of Physics.* [DOI: 10.1063/1.1359150]

I. INTRODUCTION

The recent development of metal-induced crystallization (MIC) techniques represented an important breakthrough in Si technology because of considerable interest in low-temperature formation of polycrystalline Si.[1–8] In particular, MIC methods avoid problems associated with the use of low-cost and low-softening point substrates, such as glass or polymers, by reducing the crystallization temperature for a given silicon structure.

The MIC phenomenon relies on the epitaxial growth of Si crystals on the lattice-matched silicides of some transition metals, formed typically by thermal annealing of *a*-Si films either capped with a thin metal film[1,5–8] or metal implanted.[2] To date, Ni appears to be one of the best suited metals for this purpose, and silicon crystal growth on $NiSi_2$ received a substantial coverage in the literature.

The mechanism of MIC is frequently described based on the understanding of the inverse process, namely, heteroepitaxy of silicide on silicon. The epitaxial Ni silicide films on the Si substrates have been widely studied in the past two decades because of their important applications as interconnections in the integrated circuit industry. It has been clearly established that the reaction between a Ni film and a crystalline Si wafer exhibits a sequential growth of three phases.[9] The first Ni-rich phase Ni_2Si forms at the Ni–Si interface at a temperature as low as 200 °C. Further consumption of the Ni atoms in the Si layer leads to the formation of NiSi at the Ni_2Si–Si interface at temperatures of about 350 °C. Ni monosilicide is also a metastable phase and transforms to Ni disilicide, $NiSi_2$, at ~700–750 °C. The formation of Ni_2Si and its transformation into NiSi rely on the diffusion-controlled phenomena,[9] whereas the formation of $NiSi_2$ is initiated by a nucleation-controlled process.[2,10] The temperature of the Ni silicide formation between a thin Ni film and a film of amorphous silicon is noticeably lower than that of the silicide grown at the Ni-crystalline Si interface. For example, the reaction between NiSi films and *a*-Si was reported to lead to diffusion-controlled growth of $NiSi_2$ at 400 °C.[11] It was found that the diffusion coefficient for Ni in unrelaxed amorphous silicon is six to eight orders of magnitude lower than that for the interstitial diffusion of Ni in crystalline Si.[12] Accordingly, the temperature lowering can be explained by a decrease in the amount of Ni atoms at the NiSi–Si interface due to limited diffuison of Ni through *a*-Si which consequently results in a more silicon-rich phase. Annealing studies of Ni-implanted *a*-Si films confirmed the possibility of the Ni diffusion-controlled nucleation of $NiSi_2$, where the former was the only phase to form[2,13] as compared to the well-documented Ni_2Si–NiSi–$NiSi_2$ sequence for the thin-film case. In the bulk (thicker than 10 μm) Ni–Si systems, the silicide phase formation sequence was shown as Ni_3Si, Ni_5Si_2, Ni_2Si, Ni_3Si, and finally, NiSi.[9,14] The absence of some of the earlier phases in the thin-film case was explained by their kinetic instability due to a sufficiently thin diffusion zone.[15]

The structural transformations in the earlier examples have been thoroughly investigated in the Ni silicide films synthesized by long-term furnace annealing of the prefabricated Ni–Si couples. All these examples involved predeposition of amorphous Si film, thus dividing the MIC process into two steps: formation of the disorderly covalent Si bonds and their subsequent breaking and rearrangement. Therefore, MIC created a precedent for the present work on the *direct growth* of the polycrystalline silicon film on a thin Ni prelayer.[16] A scanning electron microscopy (SEM) image of the Si film deposited at 575 °C on the yttria-stabilized zirconia (YSZ) substrate selectively covered with a 25-nm-thick layer of Ni, shown in Fig. 1, demonstrates the advantages of such metal silicide induced growth or, simply, metal-induced growth (MIG) of poly-Si. The grains seen on the surface of

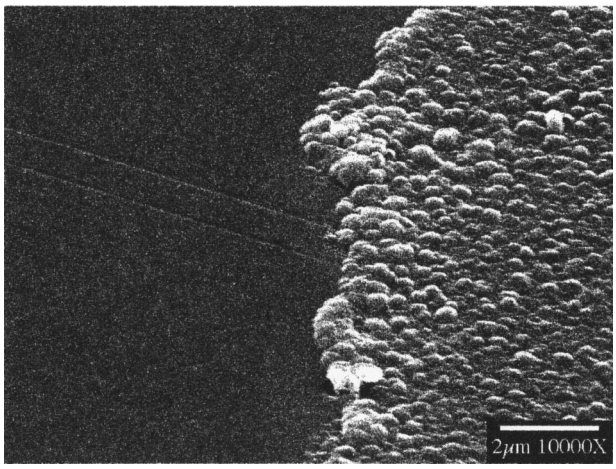

FIG. 1. A SEM image of the poly-Si thin film deposited at 575 °C on a YSZ substrate selectively covered with Ni prior to Si deposition. The polycrystalline area belongs to the film grown on a Ni underlayer.

the film belong to the area capped with Ni prior to the Si deposition, while the rest of the film is amorphous.

In the previous study,[16] we described the metal-induced grown poly-Si films in terms of their structural properties. In order to provide a better control of the MIG–Si film structure, the physical mechanisms underlying the Si crystal growth on a Ni prelayer need to be clarified. In this study, we address the dynamics of the entire process beginning with the reaction of polycrystalline Ni with sputtered Si atoms and ending with the Si grain coarsening and film growth. The MIG phenomenon will be discussed in terms of the Ni–Si interdiffusion kinetics, Ni_xSi_y phase nucleation and heteroepitaxial growth in the $Si/NiSi_2$ system.

II. EXPERIMENT

The experimental procedure has been described in detail elsewhere[16] and will be provided here only briefly. Most experiments were conducted using crystalline Si (c-Si) wafers capped with a 200–300-nm-thick plasma enhanced chemical vapor deposition silicon oxide. SiO_x-coated Corning glass slides and Mo sheets as well as YSZ crystals were also used to study the feasibility of MIG on different types of substrates. Ni films, ~25 nm thick, were deposited by Ni thermal evaporation on the above substrates at a base pressure in the low 10^{-6} Torr range. Si deposition was performed by dc magnetron sputtering from a 0.006 Ω cm phosphorus-doped Si target in a $5\%H_2/Ar$ gas mixture at a pressure of 1 mTorr. In all cases, the magnetron power was kept at 50 W while the substrate temperature was varied in the 525–600 °C range which provided a deposition rate of about 500–600 nm/h.

The x-ray photoelectron spectroscopy (XPS) analysis was performed with a Surface Science Labs model SSX-100 small spot instrument with a base pressure in the 10^{-9} Torr range. Data were obtained at an angle of 20°, using monochromatized Al $K\alpha$ radiation ($h\nu_{Al}=1487$ eV) with an x-ray spot size of 1000 μm and a source power of 300 W. Sputter depth profiles were performed with Ar ions at 4.5 keV energy with a raster area of 2 mm×2 mm, sputter time per step of ~1–2 min. The sputter rate was about 2.5 Å/s; however, it varied with the film composition. The Auger electron spectroscopy (AES) data were collected in a Physical Electronics thin film analyzer using a 5 keV incident electron beam to excite Auger electron emission. The depth profile was created using a 4 keV argon beam rastered over 3 mm×3 mm area. The Rutherford backscattering spectrometry (RBS) experiment was performed in the Dynamitron type accelerator, using a randomly aligned He^+ beam with an energy of 2 MeV and a total power of up to 30 kW. The transmission electron microscopy (TEM) analysis was carried out in a JEOL JEM 2100 high-resolution electron microscope operated at an accelerating voltage of 200 kV with a LaB_6 filament and point-to-point resolution of 1.94 Å. Selected area diffraction (SAD) was used for the phase identification of the silicide prelayer. X-ray diffraction (XRD) studies were conducted on a Phillips X'pert MPD diffractometer equipped with a Cu $K\alpha$ radiation source. SEM pictures were taken with a Hitachi S-4000 field emission scanning electron microscope operated at 20 keV in the secondary electron mode.

III. RESULTS AND DISCUSSION

A. Ni silicide formation and Ni_xSi_y phase transformations

In order to elucidate the physical mechanisms underlying the metal-induced epitaxial growth of the Si crystals on a Ni prelayer, the basic aspects of silicide formation and phase transitions need to be understood. Several methods were employed here to determine the structure, composition, and the phase changes in the silicide layer. Because these techniques were not available for *in situ* characterization, the film deposition was repeated under identical conditions and interrupted sequentially at different stages of growth. The results of the detailed investigation of thus produced films are presented below for each individual analytical method.

1. XPS depth profiling results

The samples used in the XPS studies were prepared on the 25 nm $Ni/SiO_x/c$-Si substrates at standard deposition conditions and substrate temperature of 575 °C. To obtain the first sample, silicon deposition was interrupted after 5 min in order to determine the film composition of this early stage of growth. The second sample was deposited for 1 h to study the final film structure.

The concentration variations of Si, Ni, and O across the first sample, with the thinner silicon film, are shown in Fig. 2(a). The carbon profile is not shown in the figure because its concentration was lower than the XPS sensitivity limit of 0.1%, except in the topmost 40–50 Å surface region. This ensures a low contamination of the deposited films by carbon species, which is so crucial for the electrical performance of the Si-based devices. The oxygen profile shows a concentration of about 30% on the surface, indicating that Si on the surface is partly oxidized. Initially, the oxygen peak intensity decreases with sputtering time, suggesting that with progressive depth the sample consists mostly of Ni–Si compounds. Then, the oxygen peak intensity increases again and reaches a constant value corresponding to silicon oxide of the

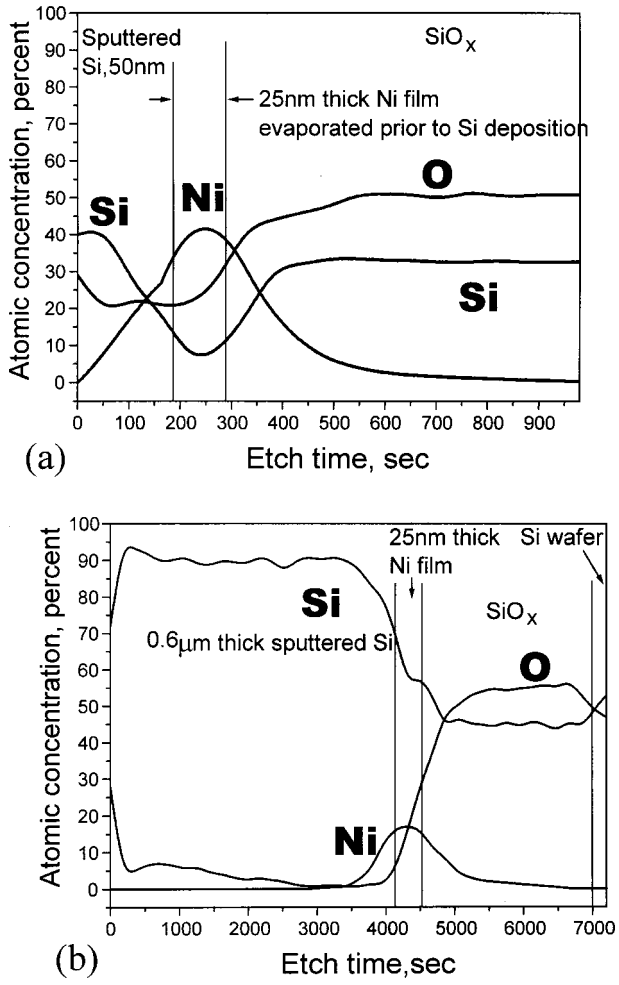

FIG. 2. XPS depth profiles of the Si films deposited for (a) 5 min and (b) 1 h at 575 °C on a 25-nm-thick Ni prelayer.

SiO_x/c-Si substrate. The most challenging task was to clarify the relationship between Si and Ni and, therefore, to provide the information about the Ni silicide phase formed first during the Si deposition on a Ni prelayer. Neither Ni nor Si profiles in Fig. 2(a) show uniform concentration across a certain thickness, suggesting that no particular phase was dominant in the sample. As seen from the depth profile, the Ni concentration gradually decreases from the bulk towards the sample surface. The Ni-to-Si concentration ratio possibly indicated Ni monosilicide (NiSi) near the Si/Ni silicide interface, and a more Ni-rich compound, such as Ni_2Si or Ni_3Si, in the region confined to the substrate. Besides, in this region, Ni partially interacts with the oxygen atoms diffused from the SiO_x layer.

Figure 2(b) shows the depth-dependent elemental profile obtained for the sample deposited for 1 h. The decrease in Si concentration with a corresponding increase in the oxygen concentration at the very surface of the Si film clearly indicates the presence of a nonstoichiometric SiO_x species (multicomponent natural oxide). The gradual increase in the oxygen atomic concentration from low levels in the deposited Si film to the stabilized 55%–60% level in the silicon oxide layer suggests that a small amount of both NiO_x and SiO_x precipitates are present in the bulk of the film. The Ni detected was confined for the most part to the region of initial Ni deposition. However, the diffusion coefficient of Ni in both crystalline Si as well as amorphous Si is known to be high at 575 °C,[12] the temperature at which the Si film was deposited. The fact that most Ni remains localized can be explained by the formation of the stable Si-rich compound, which is most likely to be Ni disilicide, known as a thermodynamically favorable Ni_xSi_y end phase. This conclusion is further supported by the average Ni-to-Si atomic concentration ratio of ~1:2 in this region.

No Ni was observed throughout the deposited Si film volume within the XPS detectability limit of 0.1%.

2. AES depth profiling results

The XPS depth profiles already showed no significant changes in the composition of the Si film near the surface, when grown for a standard time of 1 h, as seen in Fig. 2(b). Since the main phase transitions occur during the first time interval, the two samples chosen for the AES analysis, were deposited for only 4 and 12 min, respectively, with respective sample structure of a 35 nm Si/25 nm Ni/SiO_x/c-Si and a 100 nm Si/25 nm Ni/SiO_x/c-Si. The deposition temperature for these samples were kept the same as that for the samples prepared for the XPS, namely, 575 °C. In addition, one sample was prepared by depositing a 25-nm-thick Ni film on the previously obtained standard specimen (resulting in a 25 nm Ni/500 nm Si/25 nm Ni/SiO_x/c-Si) for the following reason. In this study an attempt was made to identify the phase composition by comparing the Si-to-Ni atomic concentration ratio. Most of the documented Auger standards are valid for single crystal silicon and may not apply to the micro- and poly-Si. In order to measure the Ni_xSi_y stoichiometry more precisely, the Auger depth profiles were obtained for the peak-to-peak intensity values instead of atomic concentration units. The atomic concentrations of Si and Ni were then calculated by calibrating the peak-to-peak intensities in the sample of interest against the Auger signals of pure Ni and poly-Si surfaces. On the other hand, no elemental Ni exists in the sample after the Si deposition, and a pure Ni/pure poly-Si interface can be obtained by Ni evaporation on the surface of the metal-induced grown poly-Si film with the substrate at room temperature.

The AES depth profiles for the first sample, deposited for 4 min, and the second sample, deposited for 12 min, are presented in Figs. 3(a) and 3(b), respectively. By comparison with XPS, AES appeared to be more sensitive to the presence of carbon species, indicating a 1%–2% carbon contamination in the bulk of both films, and concentration of about 20% at the very surface of the samples.

Figure 3(c) shows an Auger depth profile collected from the Ni/poly-Si standard sample, which was used to adjust the vendor supplied sensitivity factors for pure Ni and Si in order to convert raw peak intensities into atomic percents. Assuming that the plateaus in the Ni and Si signal profiles correspond to the atomic Ni and Si, the Ni:Si signal sensitivity can be found as 2.05:1 (the above ratio of Ni/c-Si is 1:2).[17] In Fig. 3(a), both Ni and Si signals increase rapidly towards the surface of the sample, stabilize at certain values, and then fall sharply at the very surface due to the carbon

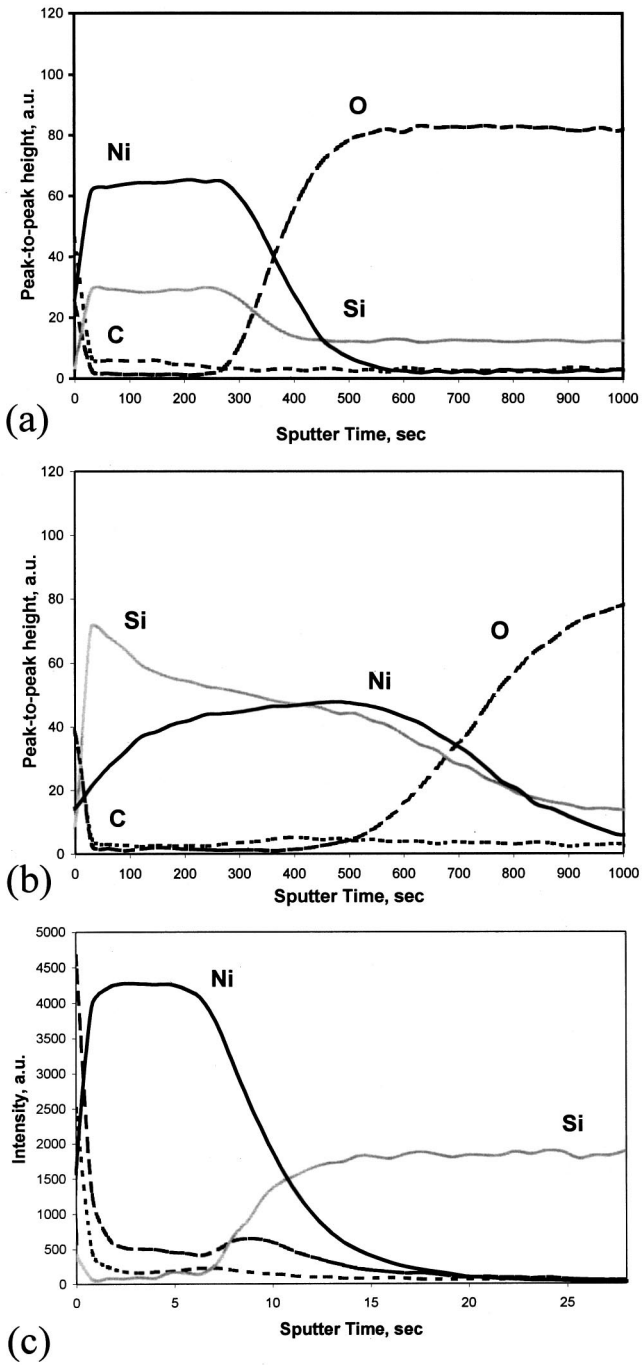

FIG. 3. AES depth profiles for (a) a 35 nm Si/25 nm Ni/SiO_x/Si sample (4 min silicon deposition); (b) a 100 nm Si/25 nm Ni/SiO_x/Si sample (12 min silicon deposition); (c) a 25 nm Ni/500 nm Si/25 nm Ni/SiO_x/Si sample used for the signal intensity calibration of elemental Ni and poly-Si.

and oxygen contamination. The fact that both Ni and Si profiles demonstrate a plateau practically over the entire sample thickness provides evidence that the film composition is invariable with depth. Using standard sensitivity factors obtained from the Ni/poly-Si sample, this composition can be calibrated as Ni:Si=1.07:1. This, in turn, might indicate the presence of at least two phases, most likely NiSi and Ni_2Si (from the above ratio, NiSi:Ni_2Si=90:10). The uniform spatial distribution of these phases seems very intriguing since it contradicts the previously proposed model in which the

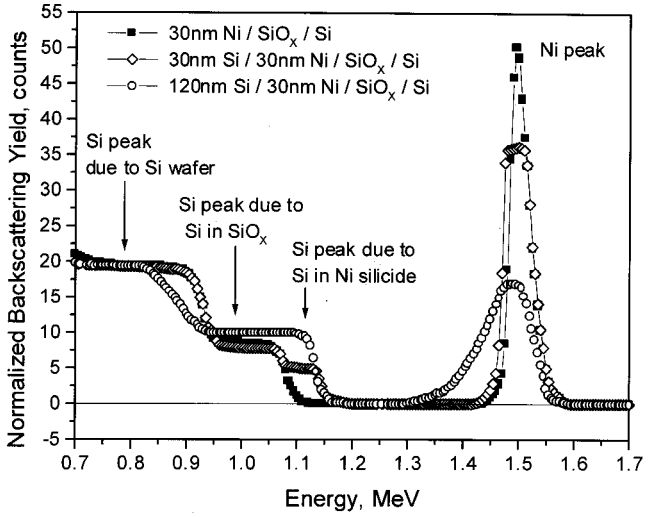

FIG. 4. RBS of a Si-on-Ni structure showing the sequential growth of Ni silicide phases. Solid symbols represent the Ni film on a SiO_x/Si substrate prior to Si deposition.

Ni_2Si–NiSi phase transition, in the Ni–Si thin-film diffusion couples, takes place exclusively at the phase interface.[18] The second sample, deposited for 12 min [Fig. 3(b)], clearly demonstrates a stratified structure, where the Ni silicide serves as an intermediate layer between the substrate and the continuously growing silicon film. These data show the silicide layer to be composed predominantly of the $NiSi_2$ crystallites. However, the accurate analysis of the Ni and Si content in Ni_xSi_y is complicated by the nonuniformity of the Ni-to-Si signal ratio distribution.

3. RBS results

For the RBS results, a 30-nm-thick Ni film was evaporated on the SiO_x/c-Si substrate. The sample was then cut into three sections. The first section was studied to provide a backscattering spectrum of a pure, unreacted nickel. The second and the third sections served as substrates for the Si films deposited at a substrate temperature of 600 °C for 3 and 15 min, respectively. The random RBS spectra of all three samples were plotted in the same figure (Fig. 4) to allow an accurate composition analysis of the formed phases.

The total energy difference ΔE between the particles scattered at the surface and near the surface is given by[19]

$$\Delta E = N\Delta x[\epsilon], \tag{1}$$

where N is the atomic density of the material (for Ni, $N=9.1\times10^{22}$ at cm^{-3}, and for Si, $N=5.0\times10^{22}$ at cm^{-3}), Δx is the penetration depth into the sample, and $[\epsilon]$ is the stopping power factor, which depends on the atomic density and the nature of the material. The stopping power factor is closely related to the stopping cross section. For the Ni_xSi_y compound, the atomic stopping cross sections can be added to give the compound stopping cross section

$$\epsilon_{\mathrm{Ni-Si}} = \frac{N_{\mathrm{Ni}}}{N_{\mathrm{Ni}}+N_{\mathrm{Si}}}\epsilon_{\mathrm{Ni}} + \frac{N_{\mathrm{Si}}}{N_{\mathrm{Ni}}+N_{\mathrm{Si}}}\epsilon_{\mathrm{Si}}, \tag{2}$$

where N_{Ni} and N_{Si} are the atomic densities in the alloy. Because the atomic concentrations are under investigation, and, hence, cannot be unambiguously determined, $[\epsilon_{Ni}]$ and $[\epsilon_{Si}]$ were considered to be equal within an accuracy of ~5%. With this assumption, the composition of the silicide layer can be given as

$$\frac{N_{Ni}}{N_{Si}} = \frac{H_{Ni}}{H_{Si}}\left\{\frac{Z_{Si}}{Z_{Ni}}\right\}^2, \tag{3}$$

where H_{Ni}/H_{Si} is the ratio of the peak heights in Fig. 4, and the atomic masses are $Z=14$ for Si and $Z=28$ for Ni.

For the second sample, the intensities of the Ni and Si peaks are 36 and 4.5 counts, respectively. Taking into account the ratio of the squared atomic masses {from Eq. (3), $[\epsilon_{Ni}]\approx[\epsilon_{Si}]$}, the composition of the film is Ni:Si $=36x(14)^2:4.5x(28)^2=2:1$. Obviously, after 3.5 min of the Si deposition, all Ni reacted with sputtered Si atoms to form Ni_2Si. Analogously, the intensities of the Ni and Si peaks in the third sample have the respective values of 16 and 10 counts, which results in the film composition Ni:Si=1:2.5. This implies that the film is composed of the Ni disilicide, $NiSi_2$, plus a small amount of elemental Si, which is caused by Si saturation in the silicide.

When the reaction between Ni and Si proceeds slowly, a coexistence of several phases (for example, elemental Ni and Ni_2Si) may be expected, which can be distinguished as a multilevel (or, multiplateau) Ni signal on the spectrum.[20,21] The RBS spectra show the absence of shoulders in either Ni or Si portions of the spectra. From the reaction rate standpoint, the absence of these ''levels'' indicates that the phase transition occurs almost instantaneously. This may also indicate that each subsequent nucleated phase grows through the thickness of the initial film as islands of a more Si-rich phase, surrounded by a uniform layer of a more Ni-rich one, instead of growing smoothly parallel to the Ni–Si interface. This interpretation is supported by the spectrum shape of the third sample, with a thicker Si film. The broadening of the Ni part of the spectrum towards low energy at the base indicates that the $NiSi_2$ grains are already formed, and extended through the whole thickness of the film.

4. TEM results

In this work, transmission electron microscopy combined with selected area electron diffraction appeared as the most powerful tool in identification of Ni_xSi_y phases, which were present in the metal-induced grown Si film. For XTEM analysis, a 25 nm thick Ni film served as a prelayer for a 500 nm thick Si film, deposited for an hour at a substrate temperature of 575 °C. A low magnification cross-sectional TEM (XTEM) image of the sample is shown in Fig. 5. Since Ni atoms are larger and, hence, less electron transparent, the dark area in the image belongs to the Ni silicide layer formed due to the reaction between Ni and sputtered Si atoms. The thickness nonuniformity of the silicide layer seen in the figure can be attributed to the morphology of isolated grains.

Figure 6(a) shows an XTEM image of the silicide layer at higher magnification followed by experimental SAD patterns [Figs. 6(b), 6(c), and 6(d)] taken in the areas identified by circles in the image. As can be concluded from Fig. 6(a), the silicide layer exhibits a stratified structure consisting of two easily identifiable regions. The top region appears lighter in the image and represents a more Si-rich silicide phase whereas the bottom section is darker and contains a higher concentration of the Ni atoms. This observation was confirmed by selected area diffraction. The top layer is found to be a pure cubic $NiSi_2$ phase ($a=5.416$ Å)[22] which provides a sufficient site for the epitaxial Si growth. As an example, a [111] SAD pattern originating from the $NiSi_2$ region is shown in Fig. 6(b). The bottom layer represents a mixture of Ni_xSi_y phases with a more Ni-rich composition. Several SAD patterns were identified with the tetragonal η-NiSi phase ($a=7.654$ Å, $c=8.4514$ Å),[23] as in Fig. 6(c). The rest of the SAD patterns [e.g., Fig. 6(d)] were consistent with the orthorhombic Ni_3Si_2 phase ($a=12.229$ Å, $b=10.805$ Å, $c=6.924$ Å).[24] Despite the fact that no other Ni_xSi_y phases

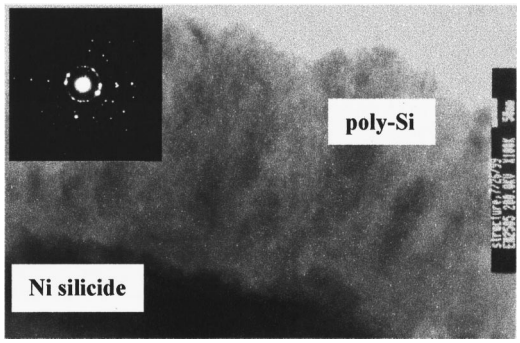

FIG. 5. (a) An XTEM image of the Si film deposited on a 25-nm-thick Ni prelayer at 575 °C; (b) SAD pattern taken at the center of the micrograph (a).

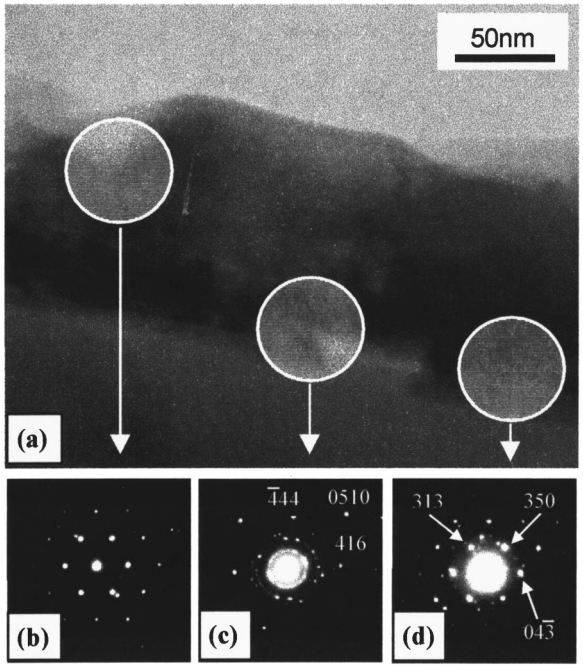

FIG. 6. (a) A higher magnification XTEM image of the Ni silicide region; (b) [111] SAD pattern corresponding to $NiSi_2$; (c) [121] diffraction pattern indicating the tetragonal NiSi phase; and (d) [534] originated from the Ni_3Si_2 phase.

were detected in the sample, their presence is possible because the capability of the SAD method may be limited by an insufficient thickness of a minor phase.

As mentioned earlier, the Ni_3Si_2 phase was not present in the case of thin-film couples. On the other hand, a fixed source of both Ni and Si exists during annealing of the predeposited thin-film couples, while in metal-induced silicon growth, the Si source is variable and increases from zero at a constant rate. Consequently, when the rate at which Si atoms arrive at the growing front is higher than that of Si diffusion into Ni, the Ni–Si interdiffusion kinetics fails to play a dominant role in silicide formation, and the latter is controlled by a Ni-to-Si concentration ratio at the interface. The most favorable $NiSi_2$ phase forms at the top of the growing film faster than might be expected in the case of ''static'' diffusion couples due to a larger number of the energetic Si atoms provided by sputtering. In $NiSi_2$, the solubility of Si in Ni reaches a limit, which prevents further diffusion of Si atoms through the $NiSi_2$ layer, and the Ni_3Si_2 stoichiometry remains unchanged.

5. XRD results

The Ni_xSi_y phases present in a series of samples deposited on a 25-nm-thick Ni film for a standard time of 1 h were also characterized by XRD. The XRD results for the samples deposited at a temperature ranging from 525 to 600 °C did not differ much qualitatively. In all x-ray scans from 2θ of 25°–60°, only three peaks are present. The peaks are observed in the vicinity of 28.5°, 47.5°, and 56.2°, as can be seen, for example, in Fig. 7(a). These diffracted intensities match the respective interplanar spacings of Si: $d=3.14$ Å (111), $d=1.92$ Å (220), and $d=1.64$ Å (311). On the other hand, due to a minor lattice mismatch, the peak positions of the corresponding diffracted planes for $NiSi_2$ are very close to those of Si. In Fig. 7(b), the XRD scan is centered around Bragg angles of 23.5°–24° (2θ=47°–48°), in the vicinity of the (220) diffracted intensity for both phases. Each of the diffuse peaks in Fig. 7(a) can be deconvoluted into two overlapping peaks, originating from Si (at smaller values of 2θ) and $NiSi_2$ (at greater values of 2θ). This result leads to two basic conclusions that Si grows epitaxially on $NiSi_2$ and that no other phase except the $NiSi_2$ is present in the sample. However, the sensitivity of the glancing angle x-ray technique is approximately 200 Å. It means that the studied silicide phase must have a thickness of over 200 Å.

Figure 7(c) shows an XRD scan of the Si film deposited at 600 °C on a 50-nm-thick Ni prelayer. The reason for preparing this particular sample, with a thicker Ni film, was to obtain a thicker silicide layer in order to thicken any minor Ni_xSi_y phases. As seen in the figure, the spectrum contains several peaks absent in the sample with a 25 nm Ni underlayer. However, these diffracted intensities could not be unambiguously assigned to a particular silicide. The structural analysis is complicated by the existence of six silicide phases below the eutectic point which possess different lattice symmetries. The phase identification conducted here relied on the previous results of the TEM analysis. Tetragonal η-NiSi and orthorhombic Ni_3Si_2 were tentatively suggested here by six and three of their dominant reflections, respectively.

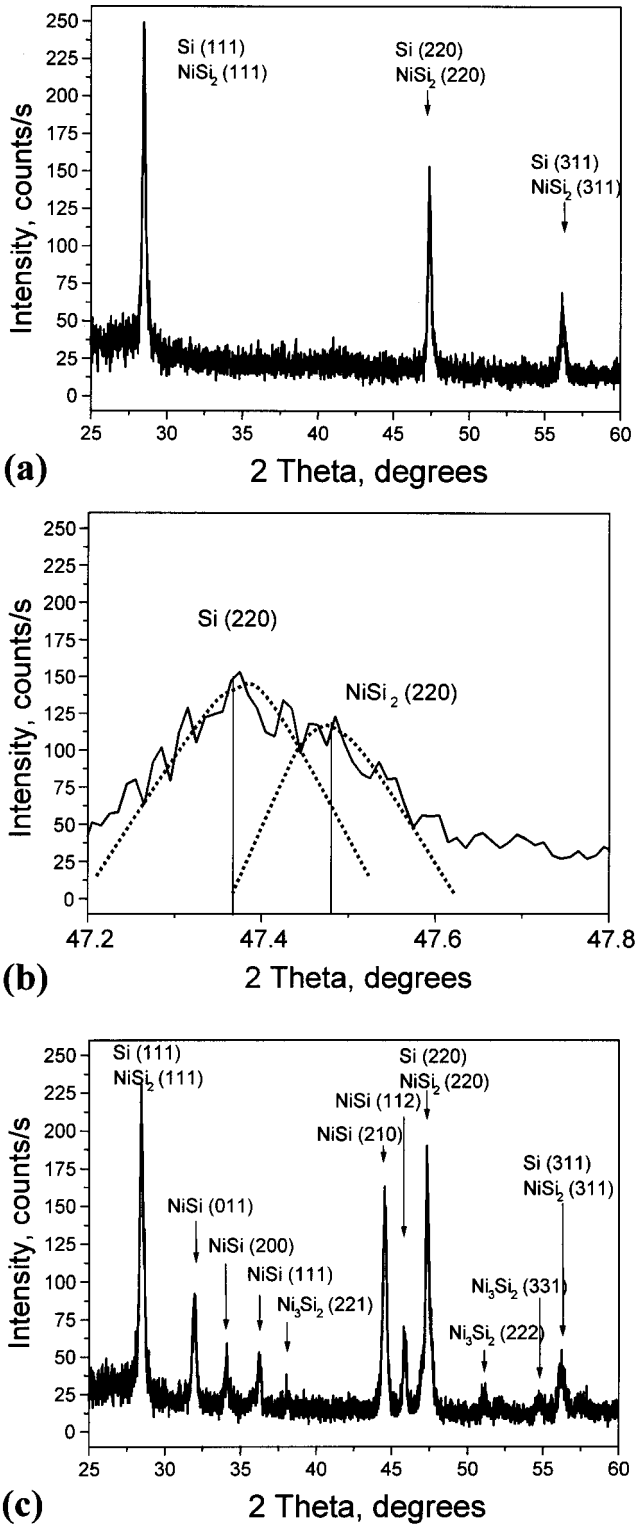

FIG. 7. (a) An XRD spectrum for the sample deposited at 600 °C on a 25-nm-thick Ni prelayer; (b) the (220) portion of the XRD spectrum in (a); and (c) an XRD spectrum of the sample deposited at 600 °C on a 50-nm-thick Ni prelayer.

B. Si nucleation on $NiSi_2$

As revealed by the XPS and AES studies of samples deposited on 25-nm-thick Ni films for different time intervals, a pure Si film begins to emerge between 5 and 12 min into the Si deposition. The same conclusion can be drawn

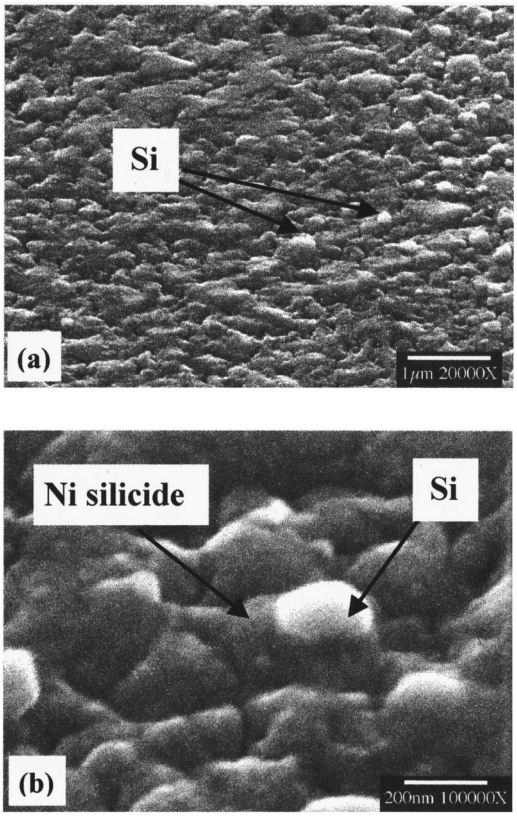

FIG. 8. A lower (a) and higher (b) magnification SEM image of a 80 nm Si/25 nm Ni/SiO_x/Si sample showing the first Si grains nucleated on the silicide surface.

from the results of the XTEM analysis, where the Si–$NiSi_2$ interface is located between 40 and 120 nm above the substrate level. In order to record the exact thickness of a Ni:Si sample at which elemental silicon starts to grow epitaxially on Ni disilicide, the surface of several samples, deposited for 5–12 min on 25 nm of Ni, was imaged using SEM.

The SEM technique was chosen for this purpose for two reasons. The first reason is that even though such dependable analytical methods as XPS and AES suggested the Si nucleation on the silicide, the visual observation of this process would provide a direct proof. Second, since SEM relies on the electron interaction, it is best suited for studying the surfaces which contain elements with different atomic masses. Therefore, silicon can be easily distinguished from the Ni silicide, which appears darker in the SEM images (as previously in TEM).

Silicon nucleation has been observed in the sample deposited for 10 min as shown in Fig. 8. The Si grains are seen to develop randomly on the sample surface. This random nucleation can be explained by a specific nonuniformity of the silicide layer, observed in TEM as well, where the first Si grains are most likely to appear in areas of Si saturation in Ni:Si.

C. Mechanistic insights into Ni-induced Si growth

Table I summarizes the changes in the Ni:Si film structure that take place during Si deposition on a Ni prelayer due to the phase transitions. The proposed mechanism of MIG is described below in accordance with new experimental findings reflected in the table.

Since Si deposition starts at the elevated substrate temperature (~525–600 °C), the very first Si atoms arriving at the substrate react with Ni, and Ni silicide begins to nucleate immediately after the onset of Si deposition due to the low activation energy of formation. Since there are fewer Si atoms available at that moment to form the silicide, as compared to a large number of the Ni atoms, the first silicide phase to appear is naturally expected to be Ni rich. In other words, while Si is consumed in Ni, metastable Ni-rich silicide initially forms and grows without any detectable changes. According to the results of XPS, AES, and RBS, this silicide represents the Ni_2Si phase. However, the results of the TEM and XRD studies do not eliminate the possibility of Ni_3Si or/and Ni_5Si_2 formation.

Continued Si deposition leads to the increased amount of Si atoms available at the silicide-silicon interface. This, in

TABLE I. Summary of the phase formation sequences in metal-induced growth of polysilicon on a Ni prelayer.

Duration of Si deposition (min)	Anticipated Si film thickness (over Ni) (nm)	Final film composition	Revealed by
3	25	Pure Ni_2Si	RBS
4	35	~90% NiSi+~10% Ni_2Si other minor phases with 1<Ni:Si<2 are possible	AES
5	45–50	NiSi+a small amount of a more Ni-rich phase (Ni_2Si or Ni_3Si)	XPS
12	100	$NiSi_2$ closer to the substrate (other minor, not Si-saturated phases are possible) +a thin layer of pure Si on the top	AES
15	120	$NiSi_2$ layer on the bottom of the sample+pure Si on the top	RBS
60 (1 h)	500–550	A thick Si film+$NiSi_2$ underlayer (+a very small amount of Ni_3Si_2 and NiSi at the very substrate)*	XPS, TEM,* XRD*

turn, results in the transformation of the Ni-rich silicide phases into the more Si-rich ones, mainly NiSi and possibly, Ni_3Si_2 (TEM, XRD). Further increase in concentration of the Si atoms at the growth front results in the formation of the most favorable phase, $NiSi_2$. The Si atoms impinging the growing film surface diffuse into the Ni film, thickening the silicide transition region until all of the Ni is consumed. Although the presence of the Ni_3Si_2 and NiSi phases in the final sample structure, revealed by TEM and XRD, is surprising, it may also be explained. Formation of the most favorable $NiSi_2$ phase on the top of the growing film is accelerated by the constantly increasing amount of the sputtered Si atoms at the surface, which makes deposition rate a parameter of primary interest. This $NiSi_2$ layer prevents further diffusion of the Si atoms due to the low Si diffusivity in $NiSi_2$, and hence, their consumption by Ni_3Si_2 and NiSi. As a result, the Ni_xSi_y composition of the silicide layer adjacent to the substrate is not altered by continued Si deposition.

In the meantime, Si atoms continue to arrive at the growth front. Since, as stated, the solubility of Si in Ni reaches a limit, the arriving Si atoms bind the already established $NiSi_2$ crystal network due to a good (0.4%) lattice match with Ni disilicide. As seen in Figs. 5, 6, and 8, the silicide layer exhibits a polycrystalline structure and, hence, irregular/uneven/rough planar morphology. The first Si grains nucleate at the sites where Si is saturated in $NiSi_2$ crystals. The grain growth then proceeds in the direction perpendicular to the $NiSi_2-Si$ interface, thereby accounting for the columnar structure of the Si film.

According to the basic theory of heteroepitaxy,[25] an epitaxial layer will grow on a lattice-matched substrate pseudomorphically, i.e., elastically strained to have the same lattice constant as the substrate, up to a certain critical thickness which is inversely proportional to the lattice mismatch between the two materials. Even such a small lattice mismatch between Si and $NiSi_2$ as 0.4% permits commensurate (lattice-strained, defect-free) epitaxy only up to several tens of atomic layers of Si. Above this thickness, the mechanical stress coupled in the Si film is released, sometimes via undesirable effects such as film breakage or spalling from the substrate surface. MIG–Si films with thickness of up to 2 μm (20,000 Å) have been studied for continuity and adhesion before and after temperature treatment, and no evidence of mechanical instability was obtained. However, a thorough look at the image in Fig. 5 helps recognize families of misfit dislocations located mostly near the grain boundaries. This essentially indicates relaxation of the strained structure via generation of dislocations, which gradually relieves mismatch until the elastic strain in the film is totally eliminated.

As a final note on metal-induced silicon growth, it is worth mentioning that continued Si deposition rapidly depletes the Ni by binding it strongly to Si atoms to form the stable $NiSi_2$ compound. This prevents further Ni diffusion in the bulk of the Si film resulting in a top Si layer essentially free from Ni, thus providing the electronic quality silicon for microelectronic devices.

IV. SUMMARY

The mechanism of metal-induced growth of polycrystalline Si thin films for microelectronic applications was studied using XPS, AES, RBS, TEM, and XRD. Silicon was deposited by sputtering from a Si target onto a 25-nm-thick Ni prelayer at a temperature of 525–600 °C and yielded a continuous uniform film. The evolution of the Ni:Si layer composition and structure was investigated by analyzing the samples grown at identical deposition parameters for different time intervals in order to identify consecutive stages of film growth.

The reaction of Ni with Si atoms results in the formation of a Ni-rich Ni silicide layer at the top of the growing film immediately after the onset of Si deposition. Continued Si deposition leads to the transformation of the Ni-rich Ni_xSi_y phases into the more Si-rich ones. The Si solubility in Ni reaches a limit in the most favorable cubic $NiSi_2$ phase which at the same time serves as an excellent site for the epitaxial Si growth due to a 0.4% lattice mismatch with Si. As a result, Si crystallizes epitaxially over the already established $NiSi_2$ crystal network, and a reasonably pure Si film emerges on the surface of Ni disilicide. The Si grains nucleated at the $NiSi_2-Si$ interface grow in the direction perpendicular to the interface providing a Si layer with a columnar structure.

ACKNOWLEDGMENTS

The authors are thankful to Dr. Castracane and Dr. Efstathiadis for the help in performing RBS and AES analysis at SUNY Albany. This research was partly funded by a NASA Space Grant through Cornell University.

[1] G. Liu and S. J. Fonash, Appl. Phys. Lett. **55**, 660 (1989).
[2] C. Hayzelden and J. L. Batstone, J. Appl. Phys. **73**, 8279 (1993).
[3] O. Schoenfeld, T. Hempel, X. Zhao, and Y. Aoyagi, Thin Solid Films **261**, 236 (1995).
[4] S. Y. Yoon, K. H. Kim, C. O. Kim, J. Y. Oh, and J. Jang, J. Appl. Phys. **82**, 5865 (1997).
[5] Z. Jin, G. A. Bhat, M. Yeung, H. S. Kwok, and M. Wong, J. Appl. Phys. **84**, 194 (1998).
[6] H. Kim, J. G. Couillard, and D. G. Ast, Appl. Phys. Lett. **72**, 803 (1998).
[7] S. Y. Yoon, J. Y. Oh, C. O. Kim, and J. Jang, J. Appl. Phys. **84**, 6463 (1998).
[8] S.-W. Lee, B.-I. Lee, T.-K. Kim, and S. K. Joo, J. Appl. Phys. **85**, 7180 (1999).
[9] K. N. Tu and J. W. Mayer, *Thin Films—Interdiffusion and Reactions* (Wiley, New York, 1978), Chap. 10, p. 359.
[10] K. N. Tu, E. Alessadrini, W. K. Chu, H. Krautle, and J. W. Mayer, Jpn. J. Appl. Phys. **13**, 669 (1974).
[11] D. J. Silversmith, D. D. Rathman, and R. W. Mountain, Thin Solid Films **93**, 413 (1982).
[12] A. Yu. Kuznetsov and B. G. Svensson, Appl. Phys. Lett. **66**, 2229 (1995).
[13] R. C. Cammarata, C. V. Thompson, and K. N. Tu, Appl. Phys. Lett. **51**, 1106 (1987).
[14] K. N. Tu, G. Ottaviani, U. Gösele, and H. Föll, J. Appl. Phys. **54**, 758 (1983).
[15] U. Gösele and K. N. Tu, J. Appl. Phys. **53**, 3252 (1982).
[16] E. Guliants and W. A. Anderson, J. Appl. Phys. **87**, 3532 (2000).
[17] K. N. Tu, W. K. Chu, and J. W. Mayer, Thin Solid Films **25**, 403 (1975).
[18] C. H. Chen, L. R. Zheng, C. B. Carter, and J. W. Mayer, J. Appl. Phys. **57**, 258 (1985).
[19] J. W. Mayer and J. M. Poate, in *Thin Films—Interdiffusion and Reactions*, edited by J. M. Poate, K. N. Tu, and J. W. Mayer (Wiley, New York, 1978).

[20] F. d'Herle, S. Petersson, L. Stolt, and B. Strizker, J. Appl. Phys. **53**, 5678 (1982).
[21] R. T. Tung and F. Schrey, Appl. Phys. Lett. **55**, 256 (1989).
[22] L. R. Zheng, L. S. Hung, and J. W. Mayer, J. Vac. Sci. Technol. A **1**, 758 (1983).
[23] A. Osawa and M. Okamoto, Sci. Rep. Tohoku Imp. Univ., Ser. 1 **27**, 341 (1939).
[24] G. Pilström, Acta Chem. Scand. (1947-1973) **15**, 893 (1961).
[25] J. W. Matthews, in *Epitaxial Growth*, edited by J. W. Matthews (Academic, New York, 1975).